Smart Structures and Systems, *Vol. 23, No. 2 (2019) 173-184*
DOI: https://doi.org/10.12989/sss.2019.23.2.173

Damage progression study in fibre reinforced concrete using acoustic emission technique

Nawal Kishor Banjara*, Saptarshi Sasmal and V. Srinivas

Special & Multifunctional Structures Laboratory (SMSL), CSIR-Structural Engineering Research Centre, Taramani, Chennai-600113, India

(Received June 16, 2017, Revised October 26, 2018, Accepted January 14, 2019)

Abstract. The main objective of this study is to evaluate the true fracture energy and monitor the damage progression in steel fibre reinforced concrete (SFRC) specimens using acoustic emission (AE) features. Four point bending test is carried out using pre-notched plain and fibre reinforced (0.5% and 1% volume fraction) - concrete under monotonic loading. AE sensors are affixed at different locations of the specimens and AE parameters such as rise time, AE energy, hits, counts, amplitude and duration etc. are obtained. Using the captured and processed AE event data, fracture process zone is identified and the true fracture energy is evaluated. The AE data is also employed for tracing the damage progression in plain and fibre reinforced concrete, using both parametric- and signal- based techniques. Hilbert - Huang transform (HHT) is used in signal based processing for evaluating instantaneous frequency of the acoustic events. It is found that the appropriately processed and carefully analyzed acoustic data is capable of providing vital information on progression of damage on different types of concrete.

Keywords: acoustic emission; fracture energy; fracture process zone; fibre reinforced concrete; wave transformation; HHT

1. Introduction

Acoustic emissions (AEs) are the stress waves produced by the sudden internal stress redistribution of the materials caused due to the changes in the internal (micro) structure of the material. Crack initiation and growth, crack opening and closure, dislocation movement, twinning, phase transformation, fibre pull-out or breakage, fibre-matrix debonding in composites etc. are few of the instances of possible causes of the change in the internal structure of material under investigation. Most of the sources of AEs are damage related (i.e., formation and propagation of cracks) and thus, the detection and monitoring of these emissions are very effective to monitoring the internal damage process.

The data collected from these acoustic emission waves in form of rise time, AE energy, hits, counts, amplitude, duration and many more as shown in Fig. 1, are used as the initial clues for the evaluation of damages in structures and matrices. Thus, AE technique involves judicious recording of generated waves by means of sensors attached to the surface and appropriate signal processing (Barsoum *et al*. 2009), as shown in Fig. 2, to extract the inherent information about the nature of source of the stress wave captured by the AE sensors.

Formation and growth of cracks are associated with the release of elastic energy in the form of acoustic emission (AE) waves. A study for characterizing the behavior of AE signals in concrete elements under flexure was carried out by Monoki *et al*. (2009). The efficacy of the AE parameters for investigating the fracture behavior of composite specimens, for assessing the locations of cracking and identifying the occurrence of de-bonding at interface between concrete and fibre-reinforced mortar layer were studied. A study on the AE behavior of steel fibre reinforced concrete under bending was carried out by Soulioti *et al*. (2009). Steel fibres of varying content were used as discrete reinforcement in concrete slabs. Influence of steel fibre on the fracture process and on the acoustic emission activities were investigated. They found that the activities related to the acoustic emission are related to the fibre content in the matrix.

Acoustic emission energy instead of amplitude associated with each of the event was used to estimate the fracture process zone in specimens made of plain concrete (Muralidhara *et al*. 2010). A methodology was proposed for identifying the fracture process zone (FPZ) in concrete using the event information. It was found that a steep increase in the cumulative AE energy of the events with respect to time can be correlated with the formation of FPZ. Studies for characterization of the acoustic emission parameters and established the correlation of the AE parameters with the fracture process in steel fibre reinforced concrete was conducted by Aggelis *et al*. (2011). Different acoustic emission indices were correlated with the accumulated damage and identified the sources of damage. The extent of damage in reinforced concrete using intensity analysis of signal obtained from acoustic emission was investigated (Basri *et al*. 2012). Absolute energy was

*Corresponding author, Scientist
E-mail: nawalkishor@serc.res.in

ISSN: 1738-1584 (Print), 1738-1991 (Online)

computed along the horizontal length of the beam and different zones were identified based on the energy release. The damage in reinforced concrete bridge beams using acoustic emission technique was identified (Vidya Sagar *et al.* 2012). A method was proposed to assess the damage in reinforced concrete (RC) bridge beams subjected to cyclic loading.

A study on evaluation of concrete fracture procedure based on acoustic emission parameters was conducted by Hu *et al.* (2013). Experimental results indicated that appropriately obtained and processed AE signal information is capable of reflecting the formation of the internal defects and cracks in the specimen. A study was carried out on in-situ condition evaluation of reinforced concrete slabs by using the acoustic signals by Benedetti and Nanni (2014). With the measurements of deflection with increment of load, a continuous AE monitoring was carried out throughout the load test. It was attempted to correlate the change in AE parameters with the extent of damage in the RC slab. Further, experimental analysis was carried out to trace the crack evolution in concrete by employing the processed signal data obtained from AE tests (Saliba *et al.* 2015). The fracture process zone (FPZ) was determined in un-notched and notched beams with different notch depths. In order to determine the FPZ, the width and length of the FPZ were estimated based on the AE source locations maps.

From the reported studies, it is found that the acoustic emission technique is being attempted to monitor the damage in concrete structures under various loading conditions. It is to emphasize that the fibre reinforced concrete provides a different fracture mechanism and damage process due to the crack bridging effect and other micro-mechanical phenomenon associated with the fibre concrete elements, which are very different from the plain concrete.

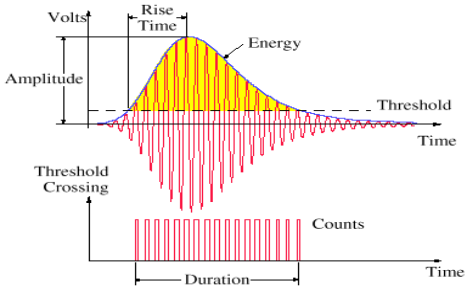

Fig. 1 AE Waveform

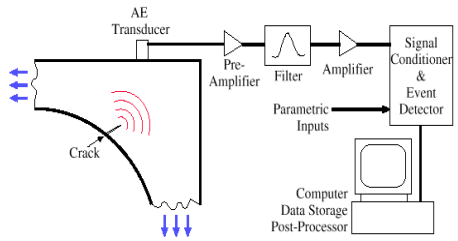

Fig. 2 AE set-up (Barsoum *et al.* 2009)

Further, though several attempts have been made to use the AE signals to monitoring the damage (mainly crack propagation) in concrete structures, works related to the characterization of stress wave exerted from the damage initiation in concrete, especially fibre reinforced concrete, is extremely scanty. In view of this, in the present study, a thorough study is carried out for evaluating the true fracture energy as well as tracing the damage process of fibre (with various volume fraction) reinforced concrete specimens using various signal parameters of AE techniques.

2. Experimental study

Plain and fibre reinforced concrete prisms of dimension 100 mm x 100 mm x 500 mm are cast for a design mix of 40 MPa concrete. For fibre reinforced concrete, two volume fraction (V_f) of hooked end steel fibre are used, as 0.5% and 1% of concrete volume with aspect ratio of 65 and length of 35 mm. The role of fibres is to arrest advancement of crack through crack-bridging effect, thus delaying the propagation of crack across the matrix which causes a delay during crack propagation. It is reported that incorporation of steel fibres in (conventional) concrete can significantly increase the tensile strength of concrete when steel fibres are used upto one percentage of volume fraction of concrete (Lee *et al.* 2004, Zaki *et al.* 2013, Banjara and Ramanjaneyulu 2018). In addition to the issues related to low workability and balling effect, the ultimate strain capacity of steel fibre cannot be fully exploited as the matrix fails in case of higher presence of fibre content in matrix. Upto a certain volume fraction of steel fibre in concrete, fracture energy increases because of debonding and pullout of the steel fibres that bridge the opening cracks. The softening behaviour of steel fibre reinforced concrete depends on the mechanical and geometrical properties of fibres as well as on the distribution and orientation of the fibres (Yoo *et al.* 2016).

2.1 Testing under monotonic load

For carrying out the fracture test, a notch of 5 mm width and 20 mm depth is created at bottom mid-span of the concrete prisms. All fracture tests are carried out using universal testing machine (UTM) with a closed-loop control system. The crack mouth opening displacement (CMOD) is measured using clip gauge of 10 mm gauge length fixed at the bottom of the concrete prism at the created notch (affixed with sharp steel holders). During the monotonic static loading, using a three point bending setup, AE signal parameters are monitored. Four wide band AE sensors of 100-1000 kHz frequency range are placed on the concrete prism as shown in Fig. 3(a). AE signals are amplified using a pre-amplifier (upto 40 dB gain). Finally, the signals are recorded by AE measurement system (SAMOS, PAC). AE waveform is recorded at 1 MHz sampling frequency. From the initial works carried out by the authors on specifying the specific acoustic characteristics of concrete, it is found that the threshold level of 45 dB is reasonable to trace the crack initiation. Hence, micro cracks having amplitudes more

than 45 dB is only captured and below which is totally ignored. Before affixing AE sensors, grease is applied as a coupling medium as an interface between AE sensors and concrete surface. Two sensors are placed at the notch level and 60 mm away from the centre and similarly two are placed 20 mm below from the top. AE sensor distribution and the test setup are shown in Fig. 3(b). Prior to the test, pencil lead break test is carried out near all the four sensors to ensure the functioning, distribution and capturing ability (distinction between noise and signal) of the wave signal.

2.2 Fracture energy based on RILEM formulation

Load - CMOD behaviour for plain and fibre reinforced concrete with different percentage of volume fraction of fibres are obtained from the experimental fracture test and as shown in Fig. 4. It is found that by adding fibres in the plain concrete, in addition to the improvement in load carrying capacity, area under the load-CMOD curve is significantly improved due to the incorporation of fibre. Fracture energy of the plain and fibre reinforced concrete (0.5% and 1%) are evaluated using Eq. (1) (RILEM, 1985).

$$G_f = \frac{\int_0^{d\delta} P(\delta)d\delta + mg\delta_0}{B(W-a_0)} \quad (1)$$

where, G_f is fracture energy, δ_0 is the value of maximum CMOD, 'mg' is the weight of concrete prism, W is width of concrete prism, H is depth of the concrete prism and a_0 is the notch length.

Fracture energy of plain concrete is found to be 126 N/m and for fibre reinforced concrete with 0.5% and 1% of fibre volume, it is found to be 190 N/m and 289 N/m, respectively. It is observed that the fracture energy is increased by 150% and 230% with respect to plain concrete by adding 0.5% and 1% volume of steel fibres (with specific geometry as used in the present study), respectively.

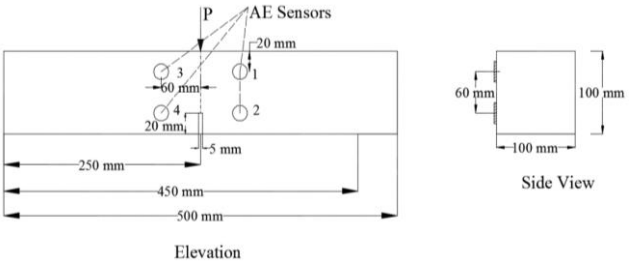

(a) Arrangement of sensors in concrete prism

(b) Test setup

Fig. 3 (a) Arrangement of sensors in concrete prism and (b) test setup

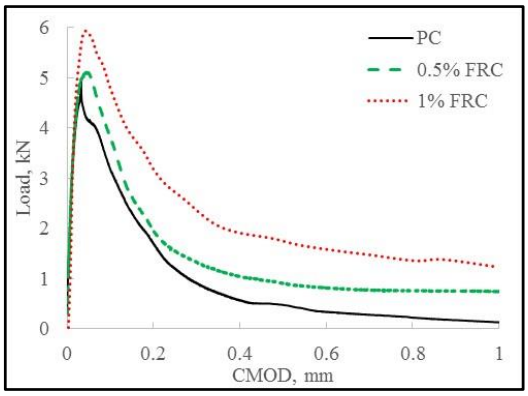

Fig. 4 Load – CMOD curve for plain concrete and fibre reinforced concrete

3. Fracture energy based on AE study

Fracture of concrete is characterized by the presence of fracture process zone (FPZ) at the crack tip, as shown in Fig. 5 (Sain and Kishen 2007, Karihaloo and Nallathambi, 1989). It is known that the effective crack length a_{eff} is longer than the true crack but shorter than the true crack plus the FPZ. The same phenomenon is more prominent for fibre reinforced concrete. Due to the presence of large number of micro cracks along the FPZ, there is a discontinuity in deformation but not in stresses. The stresses can be found as a function of the crack mouth opening displacement (CMOD). At the tip of the FPZ, tensile stress is equal to tensile strength of the concrete and it gradually reduces to zero at the tip of the true crack.

RILEM has recommended an expression for calculation of the specific fracture energy based on the work of fracture. Many researchers tried to obtain the size-independent specific fracture energy, also called true fracture energy. The size effect model based on Bazant size effect law (Bazant and Zhengzhi 1996) was adopted extensively and the fracture parameters were accordingly obtained. The boundary effect model (Kai *et al.* 2003) was able to account for the size effect of fracture energy by assuming a bi-linear variation of local fracture energy g_f over the un-notched ligament length as shown in Figure 6. The intersection of these two straight lines is defined as the transition ligament a_l^*, measured along the un-notched ligament. The relationship between local fracture energy and the size-independent fracture energy G_F was developed from the boundary effect model. Through their studies (Abdalla and Karihallo 2003) could observe that the transition ligament length first increased with an increase in the specimen size but at a reducing rate and then stabilized. The specific energy G_f according to RILEM (1985) recommendation is given in Eq. (1) which is further modified and can be written as given in Eq. (2).

$$G_f = \frac{1}{(W-a)B}\int P d\delta \quad (2)$$

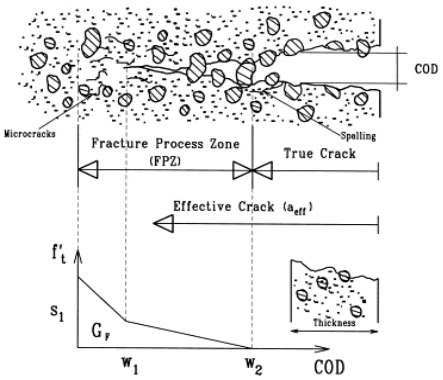

Fig. 5 Fracture process zone in concrete (Karihaloo and Nallathambi 1989)

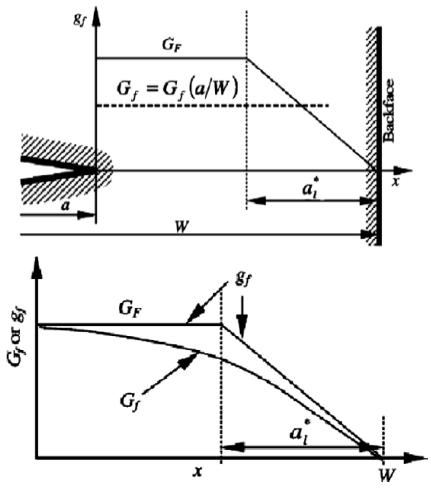

(b) Test setup

Fig. 6 Variation of local fracture energy g_f and G_f over the ligament length (Abdalla and Karihallo 2003)

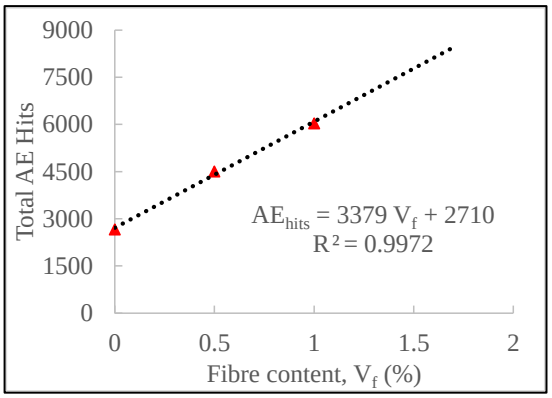

Fig. 7 Total AE hits versus fibre content

If a fictitious crack is used to model the concrete fracture, the energy dissipation for crack propagation is characterised by a cohesive stress-separation curve σ(w) which is given in Eq. (3).

$$G_f = \int_0^{w_c} \sigma(w)dw \tag{3}$$

where, w_c is the critical crack opening

Eqs. (2) and (3) mainly depends on location of fracture process zone (FPZ) in relation to the free boundary of specimen. According to energy conservation principle, specific fracture energy with size dependent, $G_f(a)$ is given in Eq. (2) is written as Eq. (4).

$$G_f(a) = \frac{1}{W-a}\int_0^{W-a} g_f(x)dx \tag{4}$$

where, $g_f(x)$ is defined as local fracture energy.

For a specimen with a ligament size (W-a) is larger than the transition ligament size a_l^*, g_f (x) can be written as given in Eq. (6).

$$g_f(x) = \begin{Bmatrix} G_F & for \quad x < (W-a-a_l^*) \\ G_F \frac{(W-a-x)}{a_l^*} & for \quad x \geq (W-a-a_l^*) \end{Bmatrix} \tag{5}$$

If (W-a) is smaller than the ligament transition length (a_l^*), G_f is obtained as given in Eq. (6).

$$G_f = \begin{Bmatrix} G_F\left[1 - \frac{a_l^*}{2(W-a)}\right] & for\ (W-a) > a_l^* \\ G_F\left[\frac{W-a}{2a_l^*}\right] & for\ (W-a) \leq a_l^* \end{Bmatrix} \tag{6}$$

where G_f is the specific or size dependent fracture energy (RILEM), G_F is the true or size-independent fracture energy, W is the overall depth of the concrete prism, 'a' is initial notch depth and a_l^* is the transition ligament length.

AE data obtained from the testing of plain concrete and fibre reinforced concrete with 0.5% and 1% of steel fibres are analysed. From the AE data, the number of AE events recorded until failure in plain concrete and in FRC with 0.5% and 1% of V_f are found to be 212, 282 and 445 respectively. AE hits are also recorded from plain concrete and FRC during testing. Almost linear relation is observed between the number of hits and the fibre content as shown in Fig. 7. This seems to be reasonable, because each fibre pull-out event is a potential AE hit and the pull-out events would increase with the fibre volume content, obviously upto an extent of volume fraction of fibre capable of taking part in crack bridging effect.

AE energy of plain concrete and FRC of 0.5% and 1%, with respect to time and channel number is plotted in Figs. 8(a)-8(c). It can be seen that crack initiates at 360, 375 and 410 seconds in plain, FRC with 0.5% and 1%, respectively. Maximum AE energy is released when crack initiates. From Figs. 9(a)-9(c), it is evident that the rate of increase of absolute AE energy is higher initially. This could be due to the formation of micro cracks at closer intervals of time. The absolute energy released from each micro crack formation in short intervals of time occurs and hence, that gives steep slope of the plot. There are some steep risers in the plot indicating high energy release rate and the formation of series of macro cracks or pull-out of fibres. The flatter portions of the plot correspond to the propagation of macro crack during which less AE energy is released. Also, with the increase in the number of micro cracks result in the reduction of stiffness and load carrying capacity which can be reflected through the increase in the number of events. Due to this obvious reasons, crack propagation in plain concrete is much faster than that in

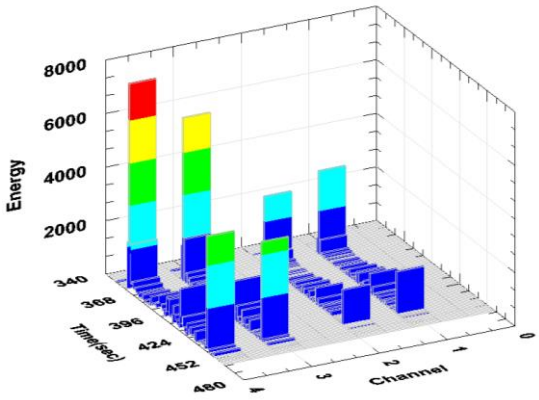

(a)

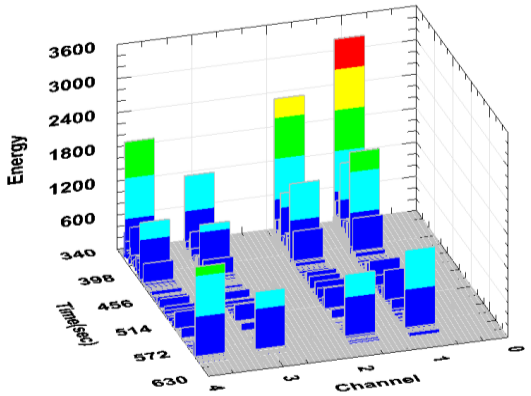

(b)

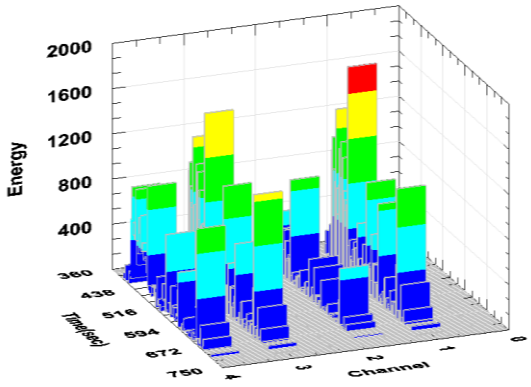

(c)

Fig. 8 AE Energy plot, (a) plain concrete, (b) FRC with 0.5% V_f and (c) FRC with 1% V_f

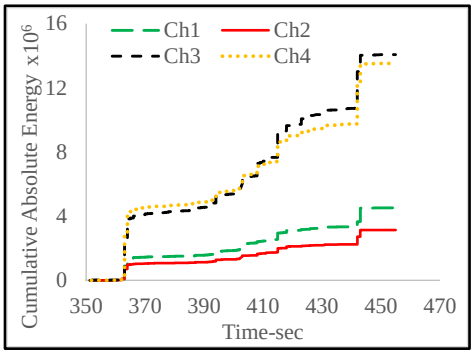

(a)

Continued-

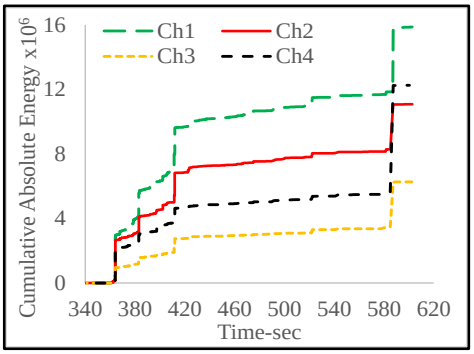

(b)

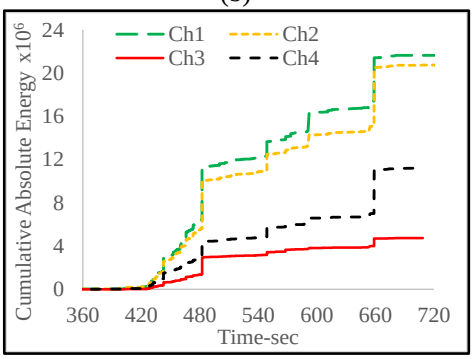

(c)

Fig. 9 Cumulative absolute AE energy plot, (a) plain concrete, (b) FRC with 0.5% V_f and (c) FRC with 1% V_f

(a)

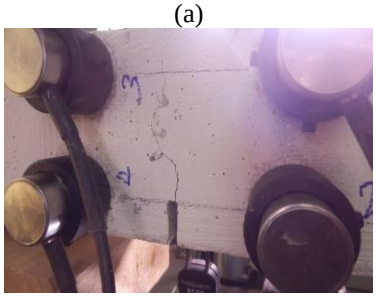

(b)

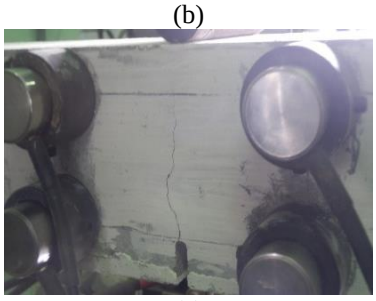

(c)

Fig. 10 Crack propagation for (a) plain concrete, (b) FRC with 0.5% V_f and (c) FRC with 1% V_f

Table 1 Total absolute energy recorded for plain concrete and FRC

Channel No	Absolute AE energy		
	Plain Concrete	FRC with 0.5% of V_f	FRC with 1% of V_f
1	4515666	**15870326**	**21649255**
2	3135830	11088081	20736521
3	**14061896**	6271671	4742586
4	13520388	12264781	11201463

FRC. Therefore, more flatter portion reflecting macro crack propagation can be observed from the AE events from FRC. The crack propagation in plain concrete and FRC are shown in Figs. 10(a)-10(c).

3.1 True fracture energy based on experimental study

Based on the AE events, true fracture energy is evaluated for plain concrete and fibre reinforced concrete with two volume fractions (0.5% and 1%) using the concept proposed for plain concrete (Muralidhara *et al*. 2010). The number of events and the total AE energy which are recorded during the test till failure of the specimen reflect the fracture process zone size. It is found that the recorded AE energy and number of events obtained from individual AE sensors are different which make the task to define the FPZ size using the AE sensor data more difficult (primarily event and energy). To overcome this difficulty, the peak absolute energy from each event, i.e. the maximum absolute AE energy recorded by any sensor in that event is considered in this study as given in Table 1. Number of AE events and the total absolute AE energy considered for analysis for evaluating true fracture energy are independent of the number of channels.

It is observed that maximum absolute AE energy recorded, by sensor number 3 for plain concrete and sensor 1 for FRC with 0.5% and 1 % of V_f (Refer Fig. 3 for sensor number). Hence, the number of events and the total absolute AE energy considered for the analysis are independent of the location of the channels. AE events during testing are recorded as shown in Fig. 11.

It is known that, with the application of load on the specimen, the number of AE events directly depends on the crack initiation and propagation. With an increase in the load, due to cracking, the number of AE events also increases and in the post-peak softening regime the event number decreases as the load reduces. During this period, the crack initiation and propagation takes place from the notch tip towards the top boundary of the concrete prism. Number of events along the depth of the specimens as recorded from the entire fracture test are plotted in histogram as shown in Figs. 12(a) to 12(c).

It is observed that the occurrence of number of AE events remain almost constant for some distance along the ligament length (a_l^*) and then, monotonically reduce as crack propagates towards the top of the concrete prism. The histogram clearly depicts the trend of energy dissipation. From Figs. 12(a)-12(c), ligament length (a_l^*) is measured.

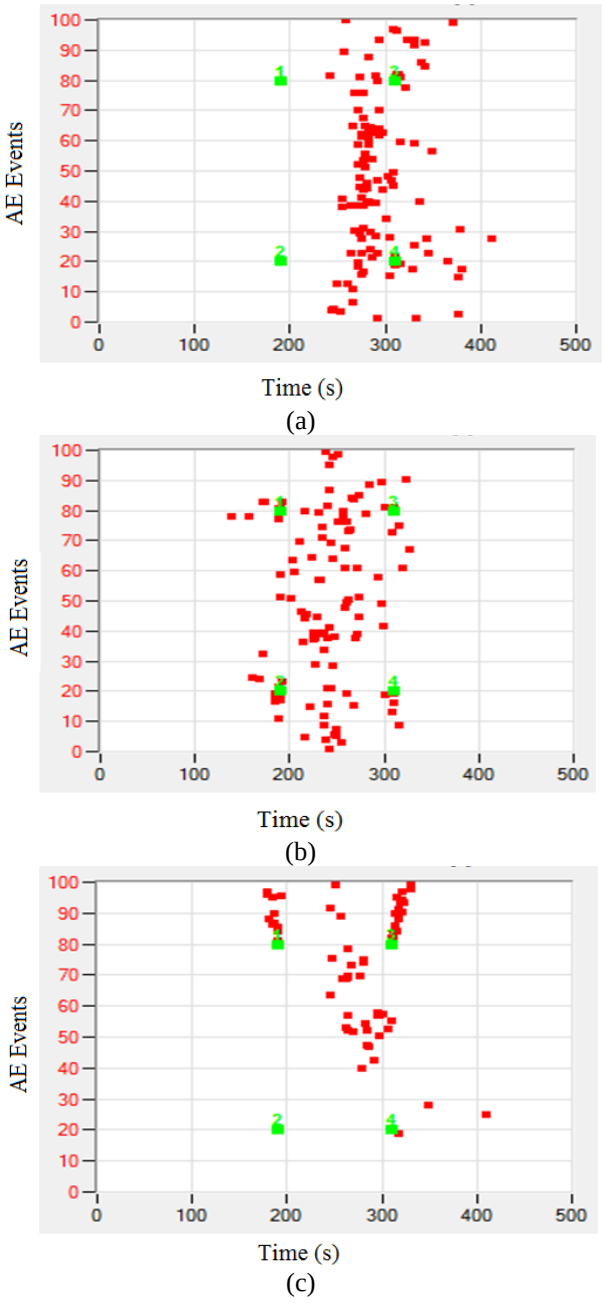

Fig. 11 AE events (x-axis (along length) and y-axis (along depth), (a) plain concrete, (b) FRC with 0.5% V_f and (c) FRC with 1% V_f

Based on Eq. (6), true fracture energy of the plain and FRC with 0.5% and 1% V_f are evaluated using measured ligament length (a_l^*) as given in Table 2. First, the fracture energy as recommended by RILEM (given in Eq. (6)) is calculated. Then based on the information on ligament length (a_l^*) derived from the acoustic emission studies, true fracture energy is calculated for different concrete and presented in Table 2. True fracture energy will be useful in understanding the fracture behaviour and damage progression of the concrete.

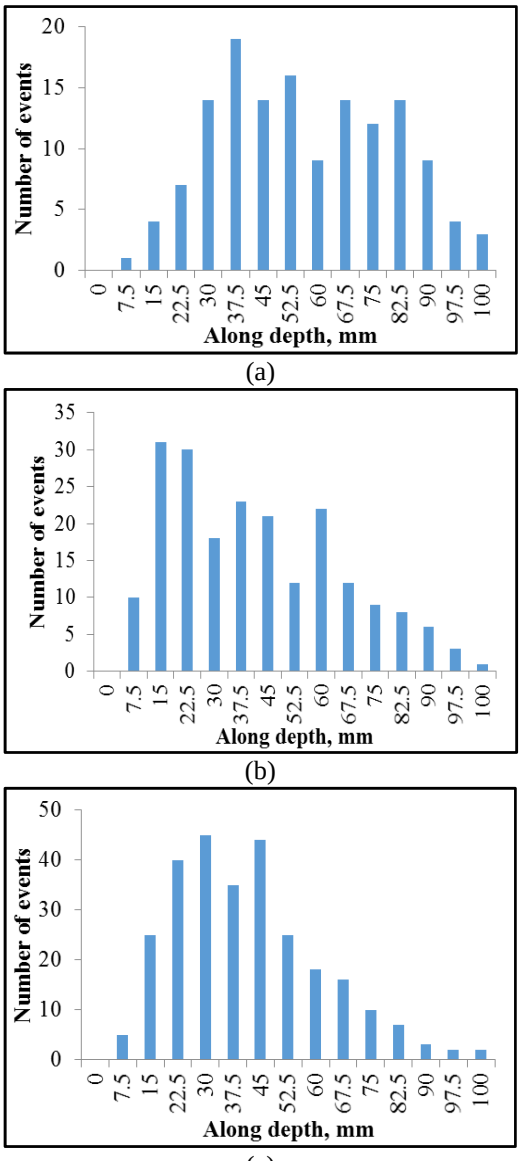

Fig. 12 Histogram of events along the ligament length (a) plain concrete, (b) FRC with 0.5% V_f and (c) FRC with 1% V_f

Table 2 Fracture energies based on RILEM and AE analysis

Specimen Name	Transition ligament length from AE data, a_l^* (mm)	RILEM fracture energy, G_f (N/m)	True fracture energy, G_F (N/m)
PC	17.5	126	142
FRC_0.5% V_f	40	190	253
FRC_1% V_f	55	289	437

3.2 Crack monitoring using digital image correlation (DIC)

For evaluation of strain state and crack propagation, Digital image correlation (DIC) technique is an extremely useful and complementary technique. It gives high resolution measurement of the surface displacement field. It works based on the conservation of the optical flow between successive images of a structure (Sutton *et al.* 1983). The planar displacement of each point of a specimen surface is computed by comparing a reference image with deformed image (Hild and Roux 2006). Based on this, the fracture lengths and the cumulative crack openings of microcracks presented in the FPZ can be easily determined (Lawler *et al.* 2001 and Alam *et al.* 2012). Aggelis *et al.* (2016) used DIC and AE to analyze the effect of reinforcement on the cracking in reinforced concrete.

In this study, to measure crack length and strain variation along the depth of the specimens, DIC is employed. A speckle pattern is applied on the specimen to facilitate the procedure of the image-processing as shown in Fig. 13(a). The region of interest is selected around the notch given, where the crack pattern needs to be studied. A reference image is taken before starting of the loading and then, images are recorded continuously at every twenty seconds during the test. Using DIC technique, strain distribution and crack width of plain and fiber reinforced concrete are studied. It is interesting to note that the distribution of strain in FRC and plain concrete specimens are very different (Figs. 13(b) and 13(c)) and as expected, strain in FRC specimen could reach a significantly higher value with long distribution. Further, DIC clearly depicts the crack bridging phenomenon in FRC specimen. It is to note that the successful crack bridging and smooth strength degradation indicate the fiber pull-out phenomenon, which is discussed in the previous section.

Further, it is important to obtain the damage responses of plain concrete and FRC based on AE studies during crack initiation and propagation. After evaluating true fracture energy, damage detection at different stages, based on captured AE data is carried out.

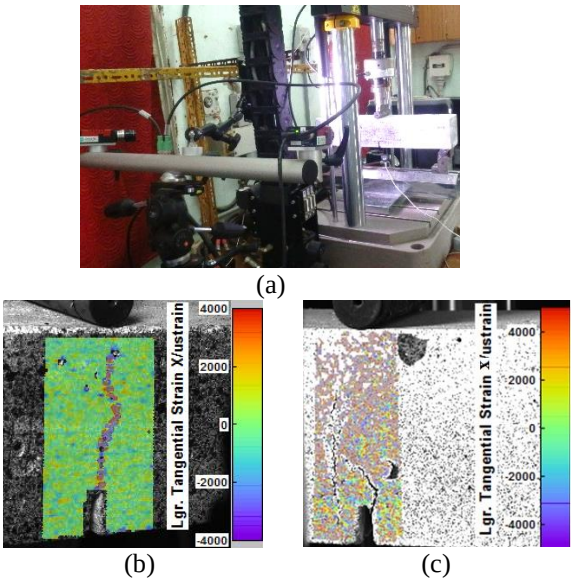

Fig. 13 (a) test set up with DIC, (b) strain distribution through the depth of plain concrete specimen and (c) strain distribution through the depth of fiber reinforced concrete specimen

4. Damage characterisation based on AE study

During the loading process without any fracture (first stage), the values of some AE parameters such as rise time, energy and amplitude are found to increase, though not significantly. However, there is obvious increment during the crack propagation (second stage) and until complete damage (third stage). As the time increased, the values of some parameters are found to have fluctuated slightly at first stage, and then kept relatively stable. At second stage, the values of some of these parameters are consistently increasing. Acoustic emission (AE) and digital image correlation (DIC) were applied during four-point bending tests on beams to follow the damage accumulation by Aggelis *et al.* (2016). AE helped to determine the onset of fracture as well as the different damage mechanisms through the registered shifts in AE rate, location of active sources and change in waveform parameters. The effect of wave propagation distance, which in components and in-situ can well mask the original information as emitted by the fracture incidents was also discussed.

The AE signals in concrete material are non-stationary random signals. In AE technique, characterizing the AE sources is most critical. In signal-based method, the feature information which can effectively reflect the damage state of structures can be judiciously extracted from AE waveform. The main objectives of time-frequency analysis are mainly to describe how the spectrum content of the signal changes with time. Most commonly used time-frequency transform methods are Wa**ve**let Transform (WT) (Yoon *et al*. 2000), Short Time Fourier Transform (STFT), Hilbert-Huang Transform (HHT) (Lu *et al*. 2011), etc. Fourier spectral analysis and wavelet are well suited for analysing data with gradual frequency changes using non-locally adaptive approach (Lin and Chu 2012). HHT is a very effective signal analysis method for non-stationary data, which was developed by Huang and Shen (2005). HHT uses the apparent time scales revealed by the signal's local maxima and minima to sequentially shift components of different time scales, starting from high to low-frequency ones. Since, HHT does not use pre-determined functions and functional orthogonality condition for component extraction, it provides considerably accurate instantaneous amplitudes and frequencies of extracted components for estimation of the system characteristics and nonlinearities (Pai and Palazoto, 2008). HHT method is used by more researchers for extraction of features from AE signal for evaluating and characterisation of damage.

HHT method to identify characteristic signal features associated with damage propagation for each failure mode in a carbon-fibre-reinforced twill-weave laminate under tensile loading was employed by Han and Zhou (2013). HHT was used to study AE signals collected from unidirectional glass-fibre reinforced polymer composites samples by Hamidi *et al.* (2013). The AE behavior of RC beams to characterize and identify different sources of damage was investigated by Gu *et al.* (2015). They proposed a mixed method in AE analysis using both parameter-based and signal-based methods. The AE signal characteristics were extracted by means of HHT which was verified as an effective method for nonlinear and non-stationary signals. However, very little, though extremely potential research on extracting the wave characteristics from AE signals using HHT is reported for concrete structures. HHT is used in the present study for extracting the AE signal parameters for damage characterisation on plain concrete and FRC with different volume fraction of fibres using parametric based and signal based method.

4.1 Concept of Hilbert-Haung Transform (HHT)

HHT mainly includes two steps: to decompose the original signal into series of Intrinsic Mode Function (IMF), and to perform the Hilbert Spectral Analysis on each IMF. The IMF which are obtained from empirical mode decomposition (EMD) must meet the following conditions: (i) the number of maximum values and minimum values are equal to the number of zero crossings; (ii) average value of upper and lower envelope should be zero at any time. Typical waveform with minima, maxima and average is as shown in Fig. 14.

The original time domain signal [x(t)] contains many IMFs. Hence, the original signal can be written as given in Eqs. (7) and (8).

$$x(t) = C_1(t) + C_2(t) + C_3(t) + \cdots + R_n(t) \tag{7}$$

$$x(t) = \sum_{k=1}^{N} C_k(t) + R_n(t) \tag{8}$$

where $C_1(t)$, $C_2(t)$ are IMFs and $R_n(t)$ is a residual from which no more IMFs can be extracted.

Further, the computed IMFs are subjected to Hilbert transformation, using the mathematical operator as given in Eq. (9). The transformed function provides a method for deconstructing both instantaneous frequency and instantaneous amplitude of the wave function, using Eqs. (10) and (11). Flow chart of HHT is shown in Fig. 15.

$$\hat{C}_k(t) = \frac{1}{\pi} PV \int_{-\infty}^{\infty} \frac{x(t')}{t - t'} dt' \tag{9}$$

where PV is Cauchy principal value.

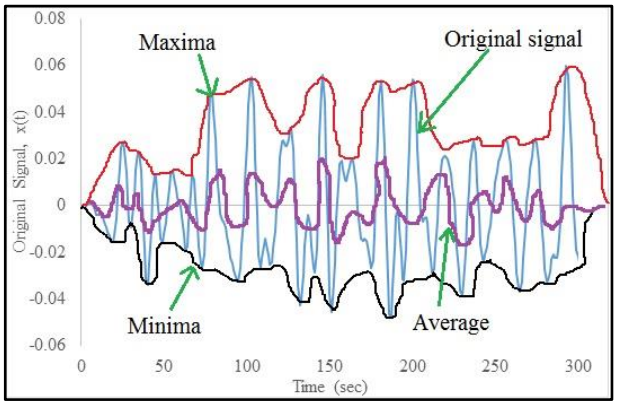

Fig. 14 Envelope of original signal, maxima, minima and average value

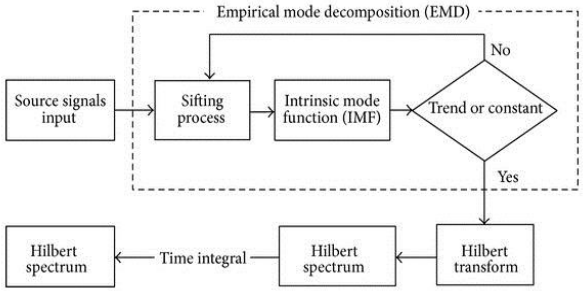

Fig. 15 Flow chart of HHT (Gu *et al*. 2015)

Then, instantaneous amplitude and frequency are given in Eqs. (10) and (11), respectively.

$$a_k(t) = \sqrt{C_k^2(t) + \hat{C}_k^2(t)} \tag{10}$$

$$f_k(t) = \frac{1}{2\pi}\frac{d}{dt}\left\{\arctan\left[-\frac{\hat{C}_k(t)}{C_k(t)}\right]\right\} \tag{11}$$

4.2 Tracing damage propagation using parametric and signal based method

Energy and cumulative signal strength (CSS) plots with respect to time are shown in Figs. 16(a)-(c) for PC and FRC. It is observed that whenever some cracks appear, there is a shift in CSS and that reflects in AE energy release. It is notable that the energy is derived from an event rather than a signal. A severe damage event always contains several signals. Due to the wide difference in magnitude of various events, the logarithm of energy named "energy magnitude" can be used as given in Eq. (12).

$$Energy\ magnitude\ = \log(E) \tag{12}$$

where E is the parameter of "AE energy" received from an AE event.

The energy magnitude of some damage events in PC and FRC are marked "A" to "H" in the energy plots (Figs. 16(a)-16(c)). These AE events occurs with maximum energy release due to cracking when load is increased. From the Figs. 16(a)-16(c), it can be found that more AE energy is released when FRC specimens are tested than plain concrete specimen. Each AE event marked in the Figs. 16(a)-16(c), has its own AE waveform signal. These AE waveform signal has different range of frequencies.

A typical AE signal extracted from an AE event is shown in Fig. 17 (say at event A). The others may be coming from successive activities or edge reflection. The AE signals with maximum energy (A to H) of plain concrete and FRC are chosen from all signals for this study. Hence, AE waveform signals of marked events (A to H), are taken for extracting frequency content. AE signal with maximum energy are separated (A to H). These AE signals contains many IMF's.

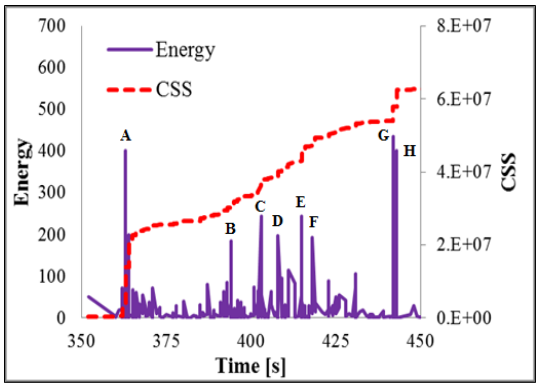

(a)

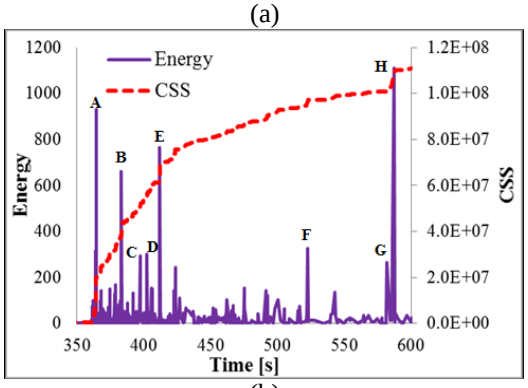

(b)

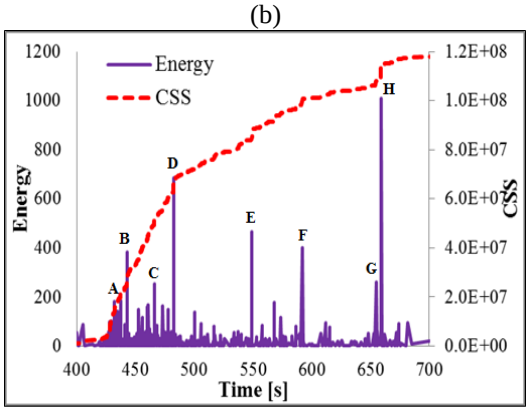

(c)

Fig. 16 AE Energy and cumulative signal strength versus time, (a) Plain concrete, (b) 0.5% FRC and (c) 1% FRC

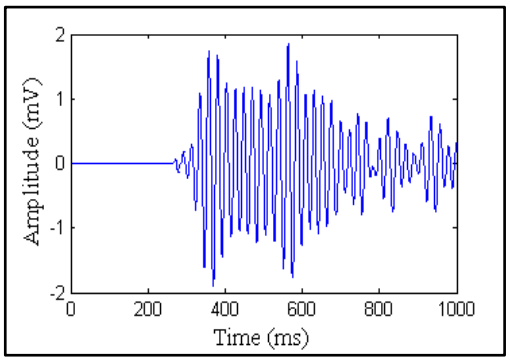

Fig. 17 Typical AE waveform signal

Table 3 Energy magnitude of obvious damage events for PC and FRC

Damage Events	PC			FRC - 0.5%			FRC - 1%		
	Time [s]	Energy Magnitude	Frequency (kHz)	Time [s]	Energy Magnitude	Frequency (kHz)	Time [s]	Energy Magnitude	Frequency (kHz)
A	363.35	2.604	215	364.18	2.968	340	431.95	2.262	130
B	394.23	2.265	130	383.07	2.819	310	442.74	2.583	180
C	402.52	2.387	145	397.39	2.468	140	465.88	2.403	150
D	408.26	2.294	125	402.32	2.480	150	482.28	2.836	240
E	415.39	2.398	130	411.93	2.884	325	548.85	2.669	175
F	417.91	2.288	120	522.48	2.515	115	592.24	2.604	170
G	441.95	2.638	250	581.94	2.425	110	654.58	2.414	135
H	442.80	2.603	240	587.38	3.045	360	658.84	3.003	375

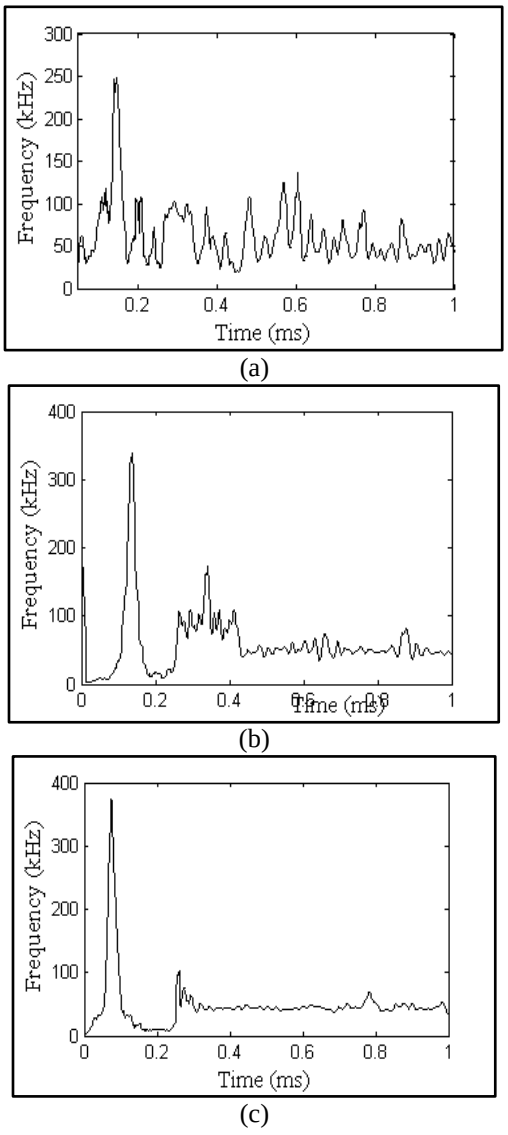

Fig. 18 Maximum frequency from HHT, (a) plain concrete, (b) FRC with 0.5% of V_f and (c) FRC with 1% of V_f (Corresponding to the maximum energy release)

Hence, first IMF's are evaluated from original wave form signals and then HHT is performed on computed IMF's. From HHT, the corresponding energy spectrum is obtained which could reveal signal features in both t ime and frequency domains simultaneously. Typical freq uency versus time are plotted for AE event of maximu m energy, i.e., damage events are A, H and H of plai n concrete and FRC, respectively as shown in Figs. 18 (a)-18(c). The corresponding instantaneous frequency wi th time at each energy peaks are extracted as given in Table 3.

Based on the signal analysis using HHT, it is observed that, in plain concrete, event 'A' is due to the sudden crack which shows higher frequency, events 'B- F' are due to crack propagation (lower frequency-almost constant) and events 'G and H' are due to failure (higher frequencies) of the concrete prism. In FRC concrete, it is seen that during initial cracking, crack propagation stage and at failure due to the pull-out of fibres, sudden release in the energy occurred which is also reflected in the form of change in the frequencies. Signal analysis in terms of energy and frequencies possesses a very regular and consistent pattern, hence can be used as failure analysis of a material/structure.

5. Conclusions

Experimental investigations were carried out on a pre-notched plain concrete and steel fibre reinforced concrete (S FRC) prism with 0.5% and 1% volume of steel fibres under monotonic loading. First fracture energy was evaluated usin g RILEM formulations. Acoustic emission technique was us ed to evaluate the true fracture energy. Based on AE event d ata, fracture process zone was defined and then true fracture energy was evaluated. For obtaining true fracture energy, li gament length is evaluated by the use of AE events. Record ed AE data were also used for damage detection in plane an d fibre reinforced concrete. Both parametric based and sign al based techniques were employed for damage detection. A n AE signal analyses approach based on Hilbert - Huang transform (HHT) was used for evaluating the instan taneous frequency. Based on the energy magnitude, damage events with more energy release were identified. Intrinsic mode functions (IMFs) were evaluated and Hilbert spectral

analysis (HAS) was performed. The change in pattern fro m signal analysis in terms of energy and frequencies a re found to be very promising for damage detection te chniques of a material/structure.

Acknowledgements

Authors acknowledge Dr. Mohit Verma, Scientist of Theoretical and Computational Mechanics Laboratory and technical staffs of Special and Multi-functional Structures Laboratory at CSIR-Structural Engineering Research Centre for providing help and support in carrying out the study.

Funding: No funding
Conflict of Interest: No conflict of interest

References

Abdalla, H. M. and Karihaloo, B.L. (2003), "Determination of size-independent specific fracture energy of concrete from three point-bend and wedge splitting tests", *Mag. Concrete Res.*, **55**(2), 133-141.

Aggelis, D.G., Soulioti, D.V., Sapouridis, N., Barkoula, N.M., Paipetis, A.S. and Matikas, T.E. (2011), "Acoustic emission characterization of the fracture process in fibre reinforced concrete", *Constr. Build. Mater.*, **25**(11), 4126-4131.

Aggelis, D.G., Verbruggen, S., Tsangouri, E., Tysmans, T. and Hemelrijck, D.V. (2016), "Monitoring the failure mechanisms of a reinforced concrete beam strengthened by textile reinforced cement using acoustic emission and digital image correlation", *Smart Struct. Syst.*, **17**(1), 91-105.

Alam, S. Y., Loukili, A. and Grondin, F. (2012), "Monitoring crack openings in concrete beams with different sizes using digital image correlation technique", *Eur. J. Environ. Civil Eng.*, **16**(7), 818-813.

Barsoum, F.F., Suleman, J., Korcak, A. and Hill, E.V.K. (2009), "Acoustic emission monitoring and fatigue life prediction in axially loaded notched steel specimens", *J. Acoust. Emission*, **27**, 40-63.

Basri, S.R., Bunnori, N.M., Abdul Kudus, S., Shahidan, S. and Jamil, M.N.M. (2012), "Evaluation of reinforced concrete damage using intensity analysis in acoustic emission technique", *Proceedings of the International Conference on System Engineering and Modeling*, IPCSIT, 34, IACSIT Press, Singapore.

Bazˇant, Z.P. and Zhengzhi, L. (1996), "Zero-Brittleness size – effect method for one-size fracture test of concrete", *J. Eng. Mech. - ASCE*, **122**, 458-468.

Benedetti, D.M. and Nanni, A. (2014), "Acoustic emission intensity analysis for in situ evaluation of reinforced concrete slabs", *J. Mater. Civil Eng. - ASCE*, **26**(1), 6-13.

Gu, A., Luo, Y. and Xu, B. (2015), "Experimental study on acoustic emission characteristics of reinforced concrete components", *Smart Struct. Syst.*, **16**(1), 67-79.

Han, W.Q. and Zhou, J.Y. (2013), "Acoustic emission characterization methods of damage modes identification on carbon fiber twill weave laminate", *Sci. China-Technol. Sci.*, **56**(9), 2228-2237.

Hamdi, S.E., Le, D.A., Simon, L., Plantier, G., Sourice, A. and Feuilloy, M. (2013), "Acoustic emission pattern recognition approach based on Hilbert-Huang transform for structural health monitoring in polymer-composite materials", *Appl. Acoust.*, **74**(5), 746-757.

Hild, F. and Roux, S. (2006), "Digital image correlation: From displacement measurement to identification of elastic properties – A review", *Strain*, **42**, 69-80.

Hu, S., Lu, J. and Xio, F. (2013), "Evaluation of fracture procedure based on acoustic emission parameters", *Constr. Build. Mater.*, **47**, 1249-1256.

Huang, N.E. and Shen, S.S.P. (2005), "Hilbert-Huang Transform and its application", Singapore, World Scientific Publishing Co. Pte. Ltd.

Kai, D., Hu, X. and Wittmann, F.H. (2003), "Boundary effect on concrete fracture and non – constant fracture energy distribution", *Eng. Fract. Mech.*, **70**(16), 2257-2268.

Karihaloo, B.L. and Nallathambi, P. (1989), "Fracture toughness of plain concrete from three-point bend specimens", *Mater. Struct.*, **22**(3), 185-193.

Lawler, J.S., Keane, D.T. and Shah, S.P. (2001), "Measuring three-dimensional damage in concrete under compression", *ACI Mater. J.*, **98**(6), 465-75.

Lee, M.K. and Barr, B.I.G. (2004), "An overview of the fatigue behavior of plain and fiber reinforced concrete", *Cement Concrete Compos.*, **26**, 299-305.

Lin, L. and Chu, F. (2012), "HHT-based AE characteristics of natural fatigue cracks in rotating shafts", *Mech. Syst. Signal Pr.*, **26**, 181-189.

Lu, C., Ding, P. and Chen, Z. (2011), "Time-frequency analysis of acoustic emission signals generated by tension damage in CFRP", *Procedia Eng.*, **23**, 210-215.

Momoki, S., Chai, H., Aggelis, D.G., Hirama, A. and Shiotani, T. (2009), "Acoustic emission for characterizing behavior of composite concrete elements under flexure", *J. Acoust. Emission*, **27**, 186-193.

Muralidhara, S., Raghu Prasad, B.K., Eskandari, H. and Karihaloo, B.L. (2010), "Fracture process zone size and true fracture energy of concrete using acoustic emission", *Constr. Build Mater.*, **24**, 479-486.

Banjara, N.K. and Ramanjaneyulu, K. (2018), "Experimental investigations and numerical simulations on the flexural fatigue behavior of plain and fiber-reinforced concrete", *J. Mater. Civil Eng. - ASCE*, **30**(8), 04018151. (DOI: 10.1061/(ASCE)MT.1943-5533.0002351)

Pai, P.F. and Palazotto, A.N. (2008), "HHT-based nonlinear signal processing method for parametric and non-parametric identification of dynamical systems", *Int. J. Mech. Sci.*, **50**(12), 1619-1635.

Rilem, T.C.S. (1985), "Determination of the fracture energy of mortar and concrete by means of three-point bend tests on notched beams", *Mater. Struct.*, **18**(106), 285-290.

Sain, T. and Kishen, J.M.C. (2007), "Prediction of fatigue strength in plain and reinforced concrete beams", *ACI Struct. J.*, **104**(5), 621-628.

Saliba, J., Loukili, A., Regoin, J. P., Grégoire, D., Verdon, L. and Pijaudier-Cabot, G. (2015). "Experimental analysis of crack evolution in concrete by the acoustic emission technique", *Frattura ed Integritá Strutturale*, **34**, 300-308.

Soulioti, D., Barkoula, N.M., Paipetis, A., Matikas, T.E., Shiotani, T. and Aggelis, D.G. (2009), "Acoustic emission behavior of steel fibre reinforced concrete under bending", *Constr. Build. Mater.*, **23**, 3532-3536.

Sutton, M.A., Wolters, W.J., Peters, W.H., Ranson, W.F. and McNeill, S. R. (1983), "Determination of displacements using an improved digital correlation method", *Image Vision Comput.*, **1**, 133-139.

Vidya Sagar, R., Raghu Prasad, B.K. and Sharma, R. (2012), "Evaluation of damage in reinforced concrete bridge beams using acoustic emission technique", *Nondestruct. Test. Evalu.*, **27**(2), 95-108.

Yoo, D.Y., Banthia, N. and Yoon, Y.S. (2016), "Predicting the flexural behavior of ultra-high-performance fiber-reinforced concrete", *Cement Concrete Compos.*, **74**, 71-87.
Yoon, D., Weiss, W. and Shah, S. (2000), "Assessing damage in corroded reinforced concrete using acoustic emission", *J. Eng. Mech. - ASCE*, **126**(3), 273-283.
Zaki, S.I., Ragab, K.S. and Eisa, A.S. (2013), "Flexural behaviour of steel fibers reinforced high strength self-compacting concrete slabs", *Int. J. Eng. Inventions*, **2**(5), 1-11.

HJ